JOC The Journal of Organic Chemistry

Article

pubs.acs.org/joc

Anthranilamides as Bioinspired Molecular Electrets: Experimental Evidence for a Permanent Ground-State Electric Dipole Moment

Bing Xia,[†,‡,#] Duoduo Bao,[†] Srigokul Upadhyayula,[†,§] Guilford Jones, II,[‡] and Valentine I. Vullev*[,†,§,∥]

[†]Department of Bioengineering, [§]Department of Biochemistry, and [∥]Department of Chemistry, University of California, Riverside, California 92521, United States

[‡]Department of Chemistry and Photonics Center, Boston University, Boston, Massachusetts 02215, United States

Supporting Information

ABSTRACT: As electrostatic equivalents of magnets, organic electrets offer unparalleled properties for impacting energy conversion and electronic applications. While biological systems have evolved to efficiently utilize protein α-helices as molecular electrets, the synthetic counterparts of these conjugates still remain largely unexplored. This paper describes a study of the electronic properties of anthranilamide oligomers, which proved to be electrets based on their intrinsic dipole moments as evident from their spectral and dielectric properties. NMR studies provided the means for estimating the direction of the intrinsic electric dipoles of these conjugates. This study sets the foundation for the development of a class of organic materials that are de novo designed from biomolecular motifs and possess unexplored electronic properties.

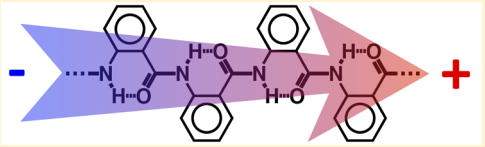

INTRODUCTION

Electrets are materials and macromolecules with ordered electric dipoles, i.e., electrets are the electrostatic analogues of magnets.[1,2] Due to the substantial electric-field gradients that their dipoles generate, electrets have an enormous potential for unprecedented applications in energy conversion, electronics, and photocatalysis applications.[3−5]

Protein helices present an important class of natural electrets. The ordered codirectional orientation of the amide and the hydrogen bonds in these protein conformers results in permanent electric dipoles amounting to about 5 debyes per residue.[6,7] For example, electric fields from protein α-helices stabilize weakly solvated ions in the interiors of the potassium, KcsA, and chloride, ClC, ion channels, permitting them to function efficiently.[8,9]

Employing polypeptide helices, derivatized with an electron donor and acceptor, Galoppini and Fox demonstrated for the first time the preferential directionality of the photoinduced electron transfer toward the positive pole of the dipole.[10,11] This charge-transfer rectification was ascribed to the stabilization of the charge-transfer states, in which the electrons were transduced toward the positive poles of the helix dipoles.[7] Employing this approach to gold interfaces coated with polypeptide helices provided a means for controlling the directionality of photocurrent.[12]

The studies described above share the corresponding electronic properties of helical peptides as the common theme for rectifying charge transfer. Indeed, these biomimetic polypeptide conjugates have proven immensely instrumental for bringing the concept of electrets to charge transfer. Such polypeptides, however, pose some challenging limitations: (1) the conformational integrity of polypeptide α-helices is often compromised when taken out of their natural environment, thus limiting the scopes of their applications,[13] and (2) polypeptides composed of natural α-amino acids are wide-band gap materials with an optical band gap of approximately 5.6 eV, which limits the distance of efficient charge transfer to less than 2 nm. Charge transfer through such polypeptides is attained solely via electron tunneling.[14−18] A hopping mechanism, involving multiple discrete electron-transfer steps along precisely arranged cofactors or redox residues, such as tryptophan, is essential for extending the charge-transfer distances beyond the intrinsic limits of the protein backbone chains.[19]

To address these issues, we undertook a bioinspired approach to attain organic electrets that have the structural and functional advantages over their biological counterparts and do not suffer the disadvantages of the biological macromolecules.[4,20] Similar to protein α-helices, we aimed at ordered amide and hydrogen bonds to generate intrinsic electric dipoles along the backbones of the bioinspired conjugates. Unlike proteins, however, our goal was to place aromatic moieties as a part of the macromolecular backbones, in order to attain extended π-conjugation and hence pathways for long-range efficient charge transfer. Anthranilamides proved to be excellent candidates for this bioinspired approach (Scheme 1).[20]

Anthranilamide oligomers are known structures existing in extended conformations stabilized by intramolecular hydrogen bonding.[21,22] In fact, anthranilic acid, i.e., *o*-aminobenzoic acid, is vitamin L_1. To date, the electronic properties of anthranilamides oligomers and their derivatives have not been

Special Issue: Howard Zimmerman Memorial Issue

Received: September 18, 2012
Published: December 27, 2012

Scheme 1. Origin of the Intrinsic Dipole Moment of Anthranilamides

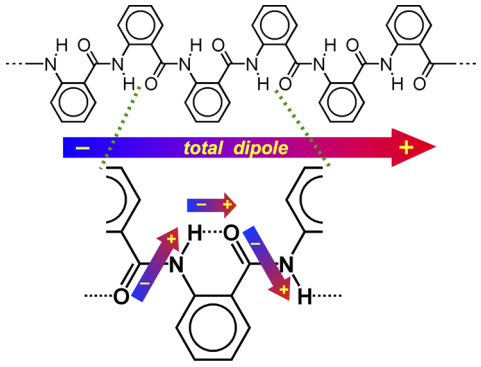

investigated. Recently, using ab initio calculations, we demonstrated for the first time that these anthranilamide oligomers have intrinsic dipole moments. The vectorial sum of the dipoles from the amide bonds, along with the dipoles generated from the shift in the electron density upon the formation of hydrogen bonds, resulted in total electric ground-state dipole moments of about 3 debyes per residue (Scheme 1).[20] Unlike in protein α-helices, the intrinsic dipoles of the anthranilamide oligomers were oriented from their N- to their C-termini (Scheme 1).[20]

Herein, we experimentally demonstrate that anthranilamides possess intrinsic dipole moments. We used relatively small conjugates, i.e., monoanthranilamide, dianthranilamide, and trianthranilamide, for this investigation (Scheme 2). Even in

Scheme 2. Anthranilamide Oligomers with Highlighted Hydrogen-Bonded (Red) and Non-Hydrogen-Bonded (Blue) Amide Protons

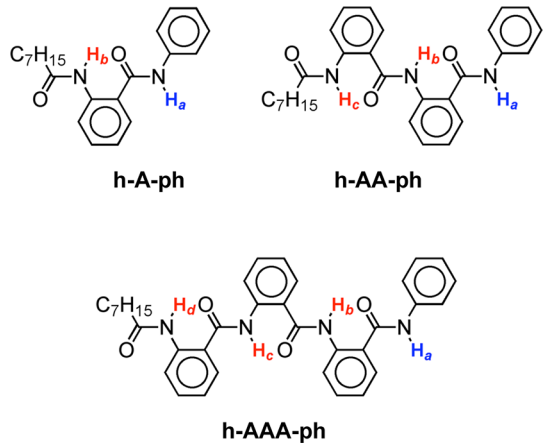

organic solvents, such as chloroform, in which these anthranilamide conjugates had pronounced solubility, they exhibited a strong propensity for aggregation. This self-assembly, however, was not electrostatically driven and the aggregates themselves had intrinsic dipoles as it became evident from dielectric studies of their solutions: i.e., at least partial codirectional arrangement of the anthranilamides within the aggregates. Analysis of ^{1}H chemical shifts, as determined using NMR spectroscopy, allowed us to determine that the direction of the intrinsic dipole was from the N- to the C-termini of the anthranilamides, which confirmed our theoretical findings.

RESULTS AND DISCUSSION

We prepared monoanthranilamide (h-A-ph), dianthranilamide (h-AA-ph), and trianthranilamide (h-AAA-ph) derivatives, in which the C-termini were capped with phenyl and the N-termini with heptyl groups (Scheme 2). For these studies, the solvent of choice was chloroform. It provided the needed sample solubility and concurrently, it was nonpolar enough to ensure that the effects from the permanent dipoles were readily detectable.[23]

Previously reported structural data indicate that anthranilamides have a preference for an extended conformation. X-ray and NMR studies demonstrated that anthranilamide oligomers assume an extended conformation with a coplanar arrangement of the aromatic rings.[21,22] Hydrogen bonding between amides attached to the same aromatic ring supports this coplanar extended conformation (Scheme 1).[21,22] Such coplanar conformations, supported by hydrogen-bond networks, are not unusual for polymers of aromatic amides and esters in organic solvents.[24−27] Furthermore, structure relaxation of a range of anthranilamide oligomers, using computational methods, constantly led to coplanar extended conformations supported by hydrogen bonds between amides attached to the same aromatic residue (Scheme 1).[20]

The UV/visible emission spectra of all three conjugates exhibited two peaks, the intensity of which was concentration dependent (Figure 1). A decrease in the concentration of these conjugates in chloroform caused a decrease in the intensity of the red-shifted band, and an increase in the intensity of the high-energy peaks. These findings were an indication for aggregation of the anthranilamides in the investigated concentration range. The emission peak at about 400 nm was due to fluorescence from the monomeric forms of the anthranilamide oligomers; and the broad band at around 520 nm was ascribed to the emission of their aggregated forms. Especially for h-AAA-ph, the intensity decrease in the aggregate emission band was less substantial than the increase in the fluorescence intensity of the 400 nm monomer emission. This finding suggested that the aggregation of the anthranilamides caused a decrease in their emission quantum yields.

Possible origins of the low energy emission band include (1) the formation of ground-state aggregates and their direct excitation and (2) excited-state aggregation (excimer formation), where photoexcited molecule aggregates with a ground-state molecule were possible origins of the aggregate emission. Close examination of the absorption spectra showed a slight increase in the extinction coefficient as the concentrations increased; a case, which was most pronounced for h-AA-ph (Figure 1a−c). These small spectral changes, however, cannot be conclusive for claiming or ruling out ground-state aggregation.

To address this issue, we resorted to time-resolved emission spectroscopy. The emission-decay curves, measured at the low-energy bands, for each of the three oligomers showed a rise within the excitation pulse, followed by immediate nanosecond decay (Figure 1d). The lack of a slow postexcitation rise (characteristic for excimer formation), along with the fast emission decay kinetics, was indicative that the low energy bands resulted primarily from ground-state aggregates.[34,35]

Addition of electrolyte and the use of a solvent media with higher polarity did not prevent the aggregation of the oligomers. Thus, electrostatic interactions (between the anthranilamide dipoles) were not the principal driving force

dx.doi.org/10.1021/jo301942g | J. Org. Chem. 2013, 78, 1994−2004

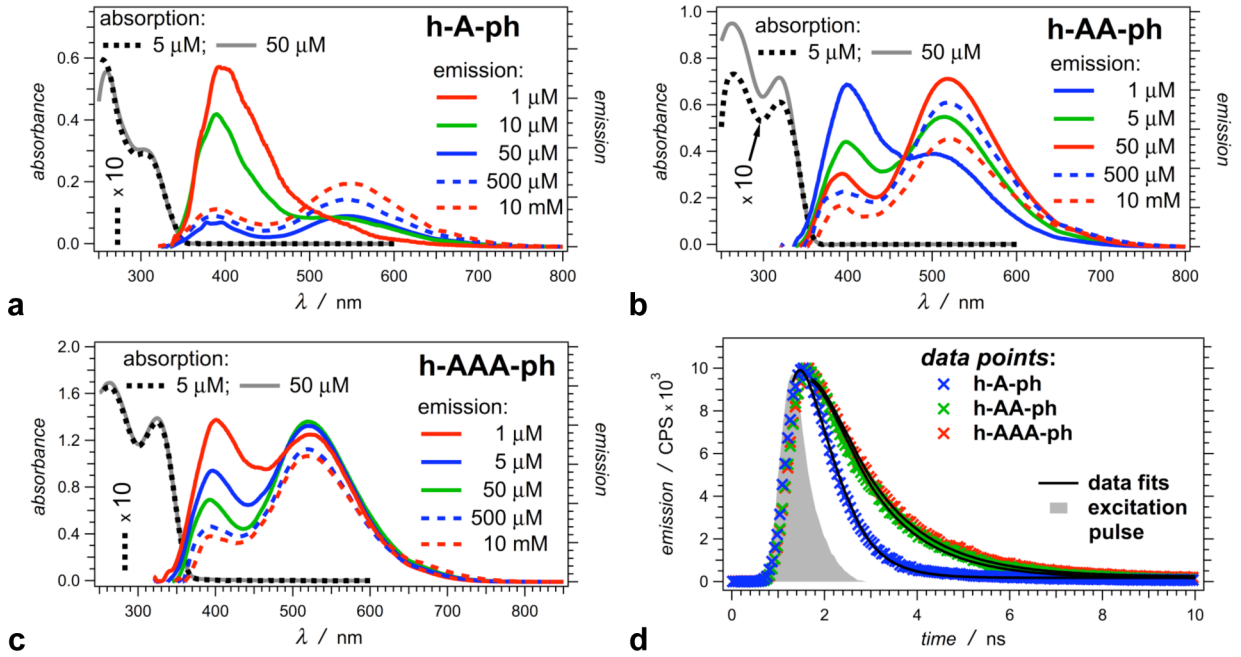

Figure 1. Absorption and emission properties of the anthranilamide oligomers. (a–c) Steady-state absorption and emission spectra (chloroform solutions; λ_{ex} = 305 nm). The absorption spectra for 5 μM concentrations were scaled up by a factor of 10 for comparison with the absorption spectra for 50 μM concentrations. The emission spectra for concentrations exceeding 10^{-4} M were recorded using small-angle fluorescence spectroscopy.[28−33] (d) Time-resolved emission decays recorded at the low-energy bands, i.e., at 545 nm for h-A-ph and at 520 nm for h-AA-ph and h-AAA-ph (λ_{ex} = 278 nm, half-height pulse width = 1 ns).

for the aggregate formation. Due to the abundance of aromatic moieties in each of the oligomers, the aggregation could be plausibly ascribed to $\pi-\pi$ stacking.

The concentration dependence of the fluorescence properties of the anthranilamides provided a means for evaluating their aggregation behavior.[37−40] Deconvolution of the fluorescence spectra (Figure 2a) allowed us to estimate the relative contribution to the emission from the monomer and the aggregate bands, i.e., R_m and R_a, respectively

$$R_m = \frac{S_m}{S_m + S_a} \tag{1a}$$

$$R_a = \frac{S_a}{S_m + S_a} \tag{1b}$$

where S_m and S_a represent the integrated emission under the monomer and aggregate bands, respectively, i.e., $S = \int F(\tilde{\nu})d\tilde{\nu}$, and $F(\tilde{\nu})$ is the fluorescence intensity at wavenumber $\tilde{\nu}$.[38,41,42]

As expected, an increase in the total concentration, C, of the anthranilamides, A, caused a decrease in S_m and an increase in S_a (Figure 2b). For h-A-ph, this change in the ratios, S, between the aggregate and monomer fluorescence bands occurred at $C < 10^{-4}$ M. For h-AA-ph and h-AAA-ph, the largest changes in S_m and S_a occurred in the sub-μM concentration range (Figure 2b).

The aggregation led to fluorescence quenching, and the emission quantum yields, Φ, of the aggregates were about 2−20 times smaller than Φ of the monomeric forms of the anthranilamides (Table 1). Therefore, R_m and R_a, as defined in eq 1, did not directly represent the equilibrium concentrations [A] and [A_n] of the anthranilamide monomers and aggregates, respectively. Considering that $S_m \propto \Phi_m$[A] and $S_a \propto \Phi_a$[A_n], along with C = [A] + n[A_n], yields

$$[A] = \frac{\phi R_m}{1 - (1 - \phi)R_m} C = \xi C \tag{2}$$

where $\phi = \Phi_a/\Phi_m$, and ξ is the fraction of the anthranilamides that are in the form of monomers, i.e., ξ = [A] / C (Figure 2c). Substituting eq 2 in the expression for the equilibrium constant, K = [A_n]/[A]^n, representing the aggregation process, nA ⇌ A_n, yields:

$$\lg(C(1 - \xi)) = n\lg(C\xi) + \lg(nK) \tag{3}$$

The slopes of the linear fits of $\lg(C(1 - \xi))$ vs $\lg(C\xi)$ provided a means for estimating of the state of aggregation, n, for the different anthranilamides (Figure 2d). For each of the anthranilamides, however, autocorrelation analysis revealed that a single linear fit over the whole concentration range did not yield statistically significant representations of the relationship between $\lg(C(1 - \xi))$ and $\lg(C\xi)$. The Durbin−Watson statistics (d) were smaller than 1 for all fits covering the full concentration ranges (Table 2),[43−46] indicating for possible positive autocorrelations that were not accounted for by the linear model, eq 3. As an alternative, linear fits limited to the concentration ranges, where the biggest changes in R_m and R_a occurred, provided excellent linear correlations with $d \approx 2$ (Table 2).

The slopes of the linear fits, limited to the low micromolar and sub-micromolar ranges, were about 1.7, 4.1, and 2.2 for h-A-ph, h-AA-ph, and h-AAA-ph, respectively (Table 2). Therefore, the observed concentration-dependent changes in the fluorescence of h-A-ph and h-AAA-ph corresponded to the formation of predominantly dimers, and of h-AA-ph tetramers. The linear fits in the concentration ranges extending to 10 mM yielded slopes of about unity, $n \approx 1$ (Table 2). Assuming that any aggregation, including between a monomer and an aggregate and between two aggregates, would affect the

dx.doi.org/10.1021/jo301942g | J. Org. Chem. 2013, 78, 1994−2004

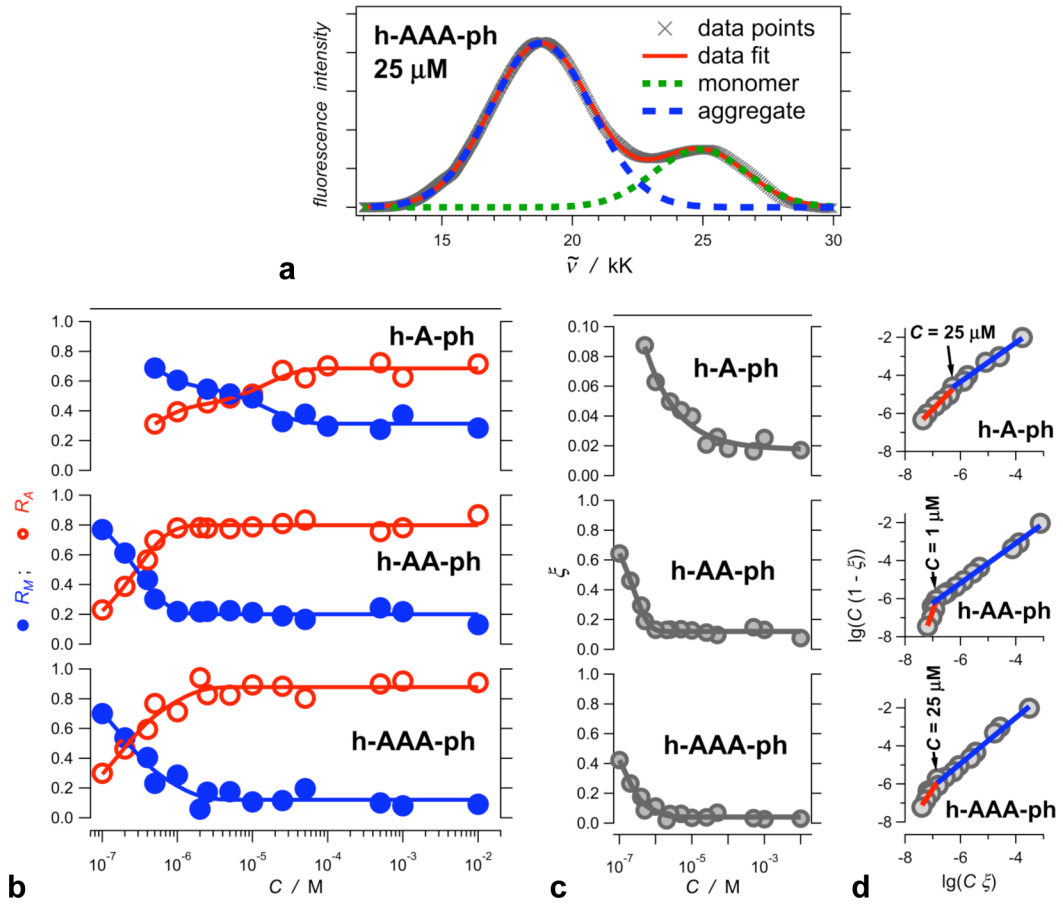

Figure 2. Concentration dependence of the emission properties of the anthranilamide oligomers. (a) Representative example of deconvolution of a fluorescence spectrum using a sum of two Gaussian functions. To plot the spectrum versus energy, i.e., vs wavenumber, $\tilde{\nu}$, instead of vs wavelength, λ, we converted the fluorescence intensity accordingly, $F\tilde{\nu}(\tilde{\nu}) = \lambda^2 F_\lambda(\lambda)$.[36] (b) Concentration dependence of the fractions of the monomer, R_m, and aggregate, R_a, emission (eq 1). (c) Concentration dependence of the monomer fractions, ξ (eq 2). (d) Linear analysis of $\lg(C(1-\xi))$ vs $\lg(C\xi)$ (eq 3). Gray circles designate the data points; red and blue lines designate the linear data fits at low and high concentrations, respectively.

Table 1. Photophysical Properties of the Anthranilamide Oligomers[a]

	λ_{abs} (nm)	ε[b] (M^{-1} cm^{-1})	λ_{em} (nm)	τ[c] (ns)	Φ_m (× 10^2)[d]	Φ_a (× 10^2)[d]	E_{00}[e] (eV)	ΔE[f] (eV)
h-A-ph	305; 260	4300	390; 545	0.594	10 ± 1	0.45 ± 0.14	3.6	4.9
h-AA-ph	320; 262	11000	400; 520	1.27	0.94 ± 0.08	0.51 ± 0.04	3.5	4.3
h-AAA-ph	325; 260	24000	400; 520	1.36	1.7 ± 0.7	0.54 ± 0.22	3.5	4.1

[a]Experimental data from UV/Visible absorption and emission measurements of chloroform solutions of anthranilamides. [b]Extinction coefficients, extrapolated to zero concentration, from nonlinear fits of the absorption at the low energy maxima (305 nm for h-A-ph, 320 nm for h-AA-ph and h-AAA-ph) vs concentration. [c]Lifetimes from time-correlated single-photon-counting measurements, samples excited at 278 nm and emission monitored at the low energy aggregate bands (545 nm for h-A-ph; and 520 nm for h-AA-ph and h-AAA-ph). [d]Φ_m and Φ_a are the emission quantum yields of monomeric and aggregated forms of the anthranilamide conjugates, respectively, obtained from extrapolation to zero and infinity concentrations. [e]Zero-to-zero energies were estimated from the cross-points of normalized absorption and emission spectra at lowest attainable concentrations. [f]Theoretically calculated HOMO−LUMO gaps, i.e., molecular "band gaps", from ref 20.

emission properties of the anthranilamides, the unity slopes for $C > 10^{-4}$ M indicated that no detectable aggregation took place in that concentration range.

The zero-to-zero energies (E_{00}),[47] extracted from the absorption and the emission spectra, correspond to the optical gaps between their highest occupied molecular orbitals (HOMOs) and their lowest unoccupied molecular orbitals (LUMOs), i.e., the optical HOMO−LUMO gaps of the anthranilamide conjugates (Table 1). The optical gaps, however, do not quantitatively represent the HOMO−LUMO energy differences. Instead, the optical HOMO−LUMO gaps of the anthranilamides characterize the direct transitions between the ground and the lowest singlet excited states, i.e., transitions that do not involve nuclear reorganization, and that are between closed-shell ground states and states with singly occupied molecular orbitals. Conversely, the calculated HOMO−LUMO gaps (ΔE) represent the theoretically estimated differences between the HOMOs and LUMOs of the ground states of the anthranilamides.[20]

For the anthranilamides, E_{00} was between 0.6 and 1.3 eV smaller than ΔE (Table 1). Two considerations could account for the differences between E_{00} and ΔE. (1) Optically determined HOMO−LUMO gaps tend to be underestimated due to the charge−charge stabilization between the electron in LUMO and the hole in the HOMO. (2) Density functional theory (DFT), which we used for calculating ΔE,[20] cannot

dx.doi.org/10.1021/jo301942g | J. Org. Chem. 2013, 78, 1994−2004

Table 2. Linear Analysis of lg($C(1-\xi)$) vs lg($C\xi$), Implementing eq 3

	fitting range[a]	n^b	d^c	accept H_0?[d]
h-A-ph	0.5 μM to 10 mM	1.29 ± 0.14	0.823	no
	0.5 μM to 25 μM	1.65 ± 0.39	2.08	yes
	25 μM to 10 mM	1.02 ± 0.16	2.36	yes
h-AA-ph	0.1 μM to 10 mM	1.27 ± 0.12	0.406	no
	0.1 μM to 1 μM	4.10 ± 0.89	1.95	yes
	1 μM to 10 mM	1.05 ± 0.07	2.01	yes
h-AAA-ph	0.1 μM to 10 mM	1.30 ± 0.11	1.02	inconclusive
	0.1 μM to 25 μM	2.16 ± 0.42	2.15	yes
	25 μM to 10 mM	1.10 ± 0.12	1.92	yes

[a]Concentration ranges of the linear fits: (1) the whole concentration range, (2) the range of low concentrations, and (3) the range of the high concentrations. [b]State of aggregation from the slopes of the linear fits (eq 3). [c]Durbin–Watson statistics: $d = (\sum_{i=1}^{n-1}\delta_{i+1} - \delta_i)^2/(\sum_{i=1}^{n}\delta_i^2)$, where δ_i are the residuals from the data fits and d can assume values between 0 and 4. Values of d close to 2 signifies no autocorrelation, d close to 0 or 4 indicates a positive or negative autocorrelation, respectively. [d]Results from testing of the null hypothesis, H_0: no autocorrelation between the residuals from the data fits. The testing of H_0 involved comparison of d with the upper and lower critical limits, $d_{U,\alpha}$ and $d_{L,\alpha}$, respectively, for $\alpha = 0.05$. If $d_{U,0.5} < d < (4 - d_{U,0.5})$, H_0 was accepted. If $d < d_{L,0.5}$ or $d > (4 - d_{L,0.5})$, the counter hypothesis was accepted. If $d_{L,0.5} \le d \le d_{U,0.5}$ or $(4 - d_{U,0.5}) \le d \le (4 - d_{L,0.5})$, the test was inconclusive.

provide feasible predictive power for the energies of unoccupied orbitals, such as LUMOs. That is, DFT can provide estimates of trends in the energies of the LUMOs within series of analogous molecules, but the absolute values of these estimates should be approached with caution.

A noticeable feature for these oligomers was the lack of considerable spectral shifts when the number of anthranilamide residues increased. While the molar extinction coefficients extrapolated to zero concentration, ε_0, increased substantially with the number of residues, the shifts in the spectral maxima did not exceed 25 nm (Table 1). In fact, the spectral maxima of h-AA-ph and h-AAA-ph were practically identical. These observations indicated that the excited states, involved in the optical transitions, were localized.[48]

To experimentally test for permanent ground-state electric dipole moments, we used the Hedestrand approach employed with the Debye solvation theory, as we have previously described.[23,49−54] Linear analysis of the concentration dependence of the dielectric constant and the density of diluted solutions of polar solutes in relatively nonpolar solvents, provides the means for estimating the molecular dipole moments of the solutes (Figure 3).[23,54,55]

In the micromolar concentration range, required for this set of studies, the anthranilamides existed as aggregates. Nevertheless, an increase in the concentration of the anthranilamides caused an increase in the dielectric constant of the chloroform solutions as determined at different frequencies from capacitance measurements with a three-terminal cell (Figure 3b,c).[54] Because only small fraction of the anthranilamides existed as monomers at concentrations exceeding about 0.5 mM (Figure 2c), the observed increase in the dielectric constant was ascribed to permanent dipole moments of the aggregates. That is, the aggregation did not cancel the permanent dipoles of these conjugates, indicating that they assembled, at least partially, in a codirectional manner.

Using the Hedestrand approach, we extracted the molar polarizations, P_{2H} (per mole oligomer), from the experimental measurements that revealed the effect of the dipole moments on the dielectric properties of the solutions (Table 3). For comparison, we calculated the orientation polarization, $P_{2\mu}$, from the theoretically determined values of the dipole moments, μ_0, of similar anthranilamide oligomers in gas phase (Table 3).[20] The magnitude of the measured polar-

Table 3. Measured and Calculated Molar Polarizations, P_2, of the Anthranilamide Oligomers

	$P_{2H}{}^a$ (cm^3 mol^{-1})	$\mu_0{}^b$ (D)	$P_{2\mu}{}^{(0)c}$ (cm^3 mol^{-1})
h-A-ph	580 ± 90	4.5	421
h-AA-ph	800 ± 50	7.5	1170
h-AAA-ph	1020 ± 310	10	2080

[a]Experimental estimated polarizations, using Hedestrand (H) approach, from dielectric and density data for chloroform solutions of anthranilamides. The values are reported per mole of oligomer.[23,57] [b]Theoretically calculated dipole moments for gas phase from ref 20. [c]Theoretically obtained orientation polarization, $P\mu$, from the calculated dipole moments: $P_{2\mu}{}^{(0)} = \mu_0{}^2 N_A/9\varepsilon_0 k_B T$.[23]

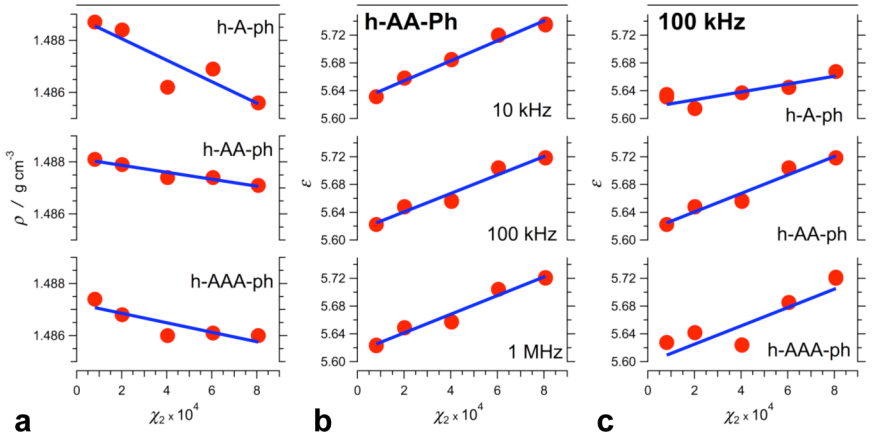

Figure 3. Dependence of (a) the density, ρ, and (b, c) the dielectric properties of anthranilamide solutions in chloroform on the oligomer molar fraction, χ_2. (b) Dielectric constant, ε, of h-AA-ph solutions extracted from capacitance measurements at different frequencies. (c) ε of solutions of the three oligomers extracted from capacitance measurements at 100 kHz.

dx.doi.org/10.1021/jo301942g | J. Org. Chem. 2013, 78, 1994−2004

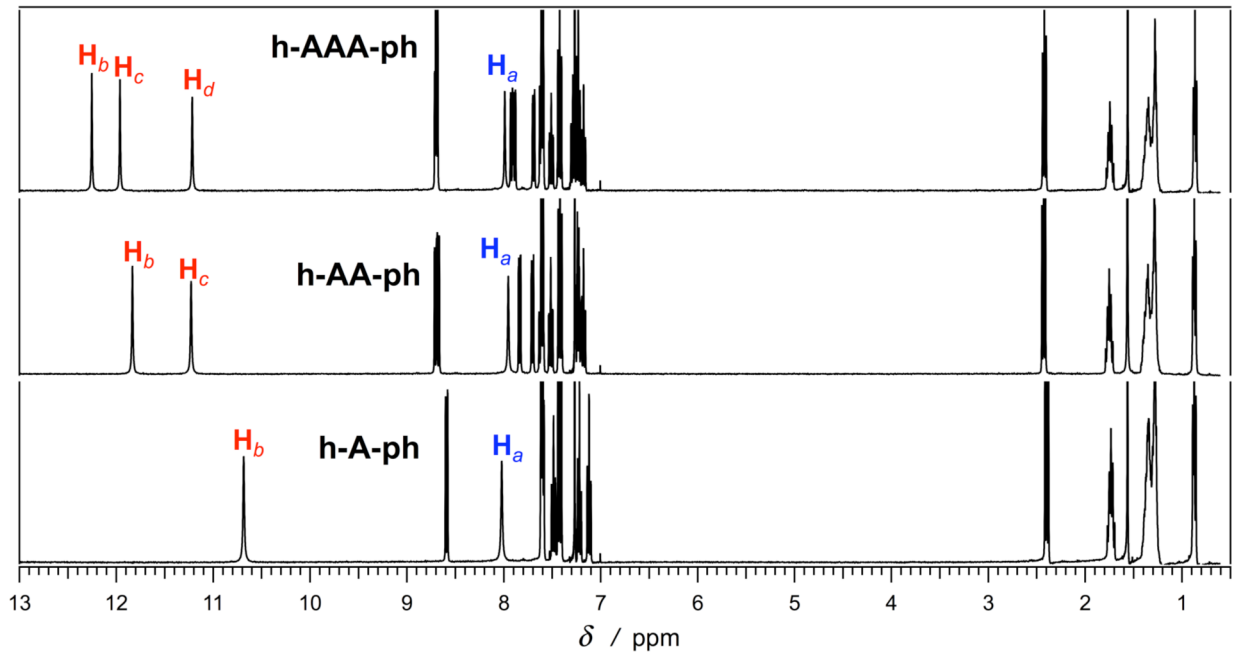

Figure 4. ^{1}H NMR spectra of the three anthranilamide oligomers with assignments of the peaks corresponding to the amide protons (2 mM in $CDCl_3$; 400 MHz).

ization, P_{2H}, indeed, increased with an increase in the oligomer size, and theoretically predicted $P_{2\mu}$ followed the same trend.

Although a fraction of the anthranilamides existed as monomers in the millimolar concentration range of the dielectric measurements (Figure 2c),[56] we could not ascribe the experimentally obtained polarizations, P_{2H}, solely to the dipoles of the nonaggregated oligomer molecules that were free in solution. Assuming that the oligomer aggregates did not have ground-state dipoles and considering the fractions of the monomers, ξ, we estimated that the measured polarizations, P_{2H}, should result in dipole values of 38, 22, and 34 D for h-A-ph, h-AA-ph, and h-AAA-ph, respectively, which were unfeasibly large, exceeding about 3 to 9 times the theoretically determined dipoles, μ_0 (Table 3). Conversely, assuming that the dipoles of the monomeric anthranilamide derivatives had values close to the theoretically estimated values of μ_0, we estimated that the nonaggregated oligomers contributed about 1.4%, 11%, and 8.5% of the measured polarizations, P_{2H}, of A-ph, h-AA-ph, and h-AAA-ph, respectively. Therefore, it was the dipole moments of the aggregates that predominantly contributed to the experimentally determined polarizations, P_{2H}.

For h-A-ph, the experimentally obtained value of P_{2H} was slightly higher than $P_{2\mu}$ (Table 3). In the mM concentration range of the dielectric measurements only about 2% of h-A-ph existed as a monomer (Figure 2c), and indeed it was the aggregate that contributed to the dielectric properties of the solutions. Considering the dimerization behavior of h-A-ph (Table 2), we estimated that the permanent dipole moment of its aggregate was 7.5 D. Assuming that each anthranilamide molecule contributes about 4.5 D to the aggregate total dipoles (Table 3), the maximum dipole expected for these dimers was 9 D. That is, the experimentally obtained value was about 83% of the theoretically expected maximum value for the dimers, indicating that h-A-ph has a strong preference for aggregating in a codirectional manner.

This propensity for codirectional self-assembly of h-A-ph could be ascribed to the asymmetry in the terminal capping groups. Upon dimerization the C-terminal phenyl would have stronger aggregation propensity with another aromatic moiety, due to $\pi-\pi$ stacking, for example, rather than for the N-terminal heptyl. Similarly, the N-terminal heptyl group would have a stronger propensity for aggregating with another alkyl, rather than with an aromatic moiety.

Considering that h-AA-ph exhibited an aggregation behavior leading to tetramers (Figure 2d, Table 2), from the measured polarization we estimated the dipole moment of its aggregate to be in the order of 13 D. Based on the calculated μ_0, the maximum possible value of the dipole of h-AA-ph tetramers was about 30 D. Similarly, the estimated value from the experimentally measured polarization for the dipole of the h-AAA-ph dimer was about 9.9 D, which was about half of the maximum possible value of 20 D for this aggregate, based on the theoretical estimate for μ_0 (Table 3). These findings indicated that h-AA-ph and h-AAA-ph also had propensity for aggregating in a codirectional manner that, however, was not as pronounced as the propensity exhibited by h-A-ph. The reason for this decrease in the preference of h-AA-ph and h-AAA-ph toward codirectional aggregation could be ascribed to the increase in their size. The larger number of aromatic rings in the longer oligomers would provide a means for more interactions between aromatic moieties, decreasing the relative contribution of the N-terminal heptyls toward the aggregation interactions, and hence decreasing the preference for the N-termini to aggregate with the N-termini of the other molecules, and the C-termini with C-termini.

Trends in the deshielding of the amide protons, $H^{(N)}$, as observed from their NMR chemical shifts, provided a means for estimation of the orientation of the anthranilamide dipoles. The C-terminal amide protons, H_a, which were not hydrogen-bonded, exhibited chemical shifts in the "aromatic" region, i.e., about 8 ppm (Figure 4). The hydrogen bonding of the rest of the amide protons, H_b, H_c, and H_d, caused deshielding and a

dx.doi.org/10.1021/jo301942g | J. Org. Chem. 2013, 78, 1994−2004

downfield shift in their signals, placing them in the "acid" region between 10.5 and 12.5 ppm (Figure 4).

Although at the concentrations we used for the NMR studies the anthranilamides existed as aggregates, each of the amide protons exhibited a single peak with a narrow Lorentzian shape. Two-dimensional (2D) NMR experiments utilizing intramolecular couplings revealed that each of these different singlets exhibited different correlation patterns, indicating that each of the peaks corresponded to only one amide proton. These findings suggested that the same amide proton, from the different molecules in an aggregate, had identical microenvironment.

To examine the effect of the anthranilamide intrinsic dipoles, we compared the chemical shifts of amide protons that belonged to the same molecule and that had identical bonding environment (i.e., identical within about one-residue radius comparable with the intramolecular NMR coupling effects we measured). The hydrogen-bonded amide protons, H_b and H_c of h-AAA-ph, were the choice for this comparison (Scheme 2). Both protons were in the middle of the oligomer, and each one of them was surrounded by three aromatic moieties with identical bonding pattern and orientation (Scheme 2). Despite their close similarity, H_b and H_c had distinctly different chemical shifts as evident from the three singlets separated from one another in the 11−13 ppm region (Figure 4). The difference in their chemical shifts could be ascribed to (1) effects from the permanent electric dipole moments and (2) differences in the microenvironments within the aggregates. The latter is not plausible because nonspecific aggregation is very unlikely to provide unique microenvironment for the same proton from different molecules in an aggregate. Therefore, it would be the intramolecular effects, along with the permanent electric dipoles, that govern the observed NMR chemical shifts.

To avoid ambiguities due to aggregation, we used only intramolecular correlations to assign the chemical shifts of the hydrogen-bonded amide protons, H_b, H_c, and H_d. Gradient-selected heteronuclear multiple bond correlation (gHMBC) allows for detecting $^1H-^{13}C$ coupling through several bonds, including through heteroatoms, such as the amide nitrogens.[58,59]

For acceptable signal-to-noise ratio, we carried out the other 2D NMR measurements, such as HMBC, at about 50 mM sample concentrations. The chemical shifts of all protons except H_a, did not exhibit concentration dependence in the range from about 1 to 50 mM. The shift of the non-hydrogen bonded proton, H_a, however, moved downfield by about 0.45 ppm as the concentration increased to 50 mM (Figure 4, 5). Changes in the state of aggregation should affect the chemical shifts of all protons.[34,38] H_a was the most labile proton in h-AAA-ph, making it sensitive to changes in the activity of traces of water in the deuterated chloroform upon increasing the molar fraction of the anthranilamide. Therefore, this downfield shift of the signal from H_a is not an indication for changes in the state of aggregation. This observation, along with the fluorescence concentration-dependence trends (Figure 1c), implied that the aggregation occurred in the micromolar and sub-micromolar range.

The signal from the most downfield-shifted aliphatic protons, H_e and $H_{e'}$ at 2.4 ppm (Scheme 3), correlated with only one peak in the carbonyl carbon region on the HMBC spectra (Figure 5a). This correlation allowed the assignment of the N-terminal carbonyl carbon C_d (Figure 5a). Concurrently, the N-terminal carbonyl carbon correlated with only one of the amide

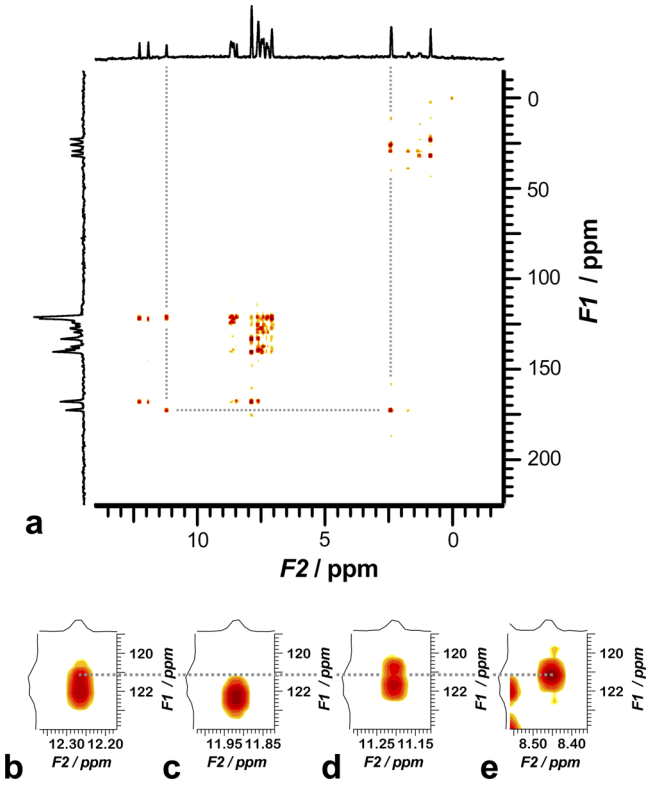

Figure 5. $^1H-^{13}C$ gHMBC spectrum of h-AAA-ph (50 mM in $CDCl_3$; 400 MHz). (a) Full spectral range with ^2J correlations (indicated with the gray lines) between $^1H_e/^1H_{e'}$ and $^{13}C_d$ and between $^{13}C_d$ and ^1H_d (Scheme 3). (b−e) Zoomed ^3J correlation peaks between the amide protons and the carbons three bonds away. Peaks at: (b) 12.3 ppm; (c) 11.9 ppm; (d) 11.2 ppm; and (e) 8.45 ppm.

Scheme 3. Trianthranilamide, h-AAA-ph, with Highlighted Protons Used for Establishing the Connectivity Patterns in the NMR Analysis

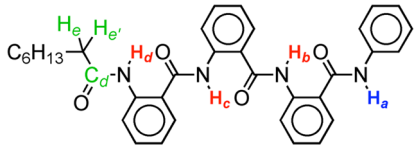

proton signals, at 11.2 ppm, which thus we assigned to H_d (Schemes 2 and 3).

To assign the chemical shifts of H_b and H_c of h-AAA-ph, we majorly resorted also to gHMBC (Figure 5). In the HMBC spectrum of h-AAA-ph, we compared the correlation peaks of the assigned terminal amide protons with the aromatic carbons in the region around 115−130 ppm (Figure 5a). The C-terminal amide proton, H_a, which was not hydrogen bonded, exhibited correlation peak with a maximum that spread between 120.9 and 121.4 ppm of the carbon shifts (Figure 5e). Concurrently, the N-terminal amide proton, H_d, exhibited two overlapping correlation peaks with maxima spreading between 120.5 and 121.0 ppm and between 121.4 and 122.0 ppm (Figure 5d).

We examined the correlation peaks from the other two amide protons for patterns of connectivity with carbons that were about three bonds away from the H_a and H_d. The correlation peak that corresponded to the amide ^1H at 11.96 ppm, had a maximum that extended between 121.9 and 122.7 ppm (Figure

dx.doi.org/10.1021/jo301942g | J. Org. Chem. 2013, 78, 1994−2004

5c). Hence, this proton had some cross-correlation overlap with H_d, i.e., the 11.96 ppm proton and H_d could be coupled to the same carbon. Concurrently, the 11.96 ppm amide proton had no cross-correlation with H_a, i.e., no common carbon to which both of them would be coupled (Figure 5c,e). Therefore, we assigned the proton at 11.96 ppm to H_c (Scheme 2, Figure 4). The amide proton at 12.25 ppm had a correlation peak with a maximum intensity that spread widely between 121.1 to 122.4 ppm over the carbon shift region (Figure 5b). This proton had cross-correlation with both H_a and with the proton at 11.96 ppm that we assigned to H_c. Conversely, due to the close overlap of the aromatic carbon peaks, we could not readily rule out cross-correlation between the 12.25-ppm proton and H_d. The lack of cross-correlation between the 11.96 ppm proton and H_a, however, made it implausible to assign the 11.96 ppm peak to H_b. Therefore, considering all possible coupling patterns, we assigned the peak at 11.96 ppm to H_c and the peak at 12.25 ppm to H_b (Figure 4).

Because everything in the bonding patterns of H_b and H_c was identical within nearest residue range, we could ascribe the difference between the chemical shifts of these two protons to effects from the local electric field generated by the anthranilamide dipole (Scheme 1). As observed for polypeptide α-helices, positive polarization from the dipole electric field lowers the pK_a of protic groups, i.e., increases their acidity and causes a downfield shift in the signals from their protons.[60] For h-AAA-ph, H_b is the most downfield shifted proton, i.e., about 0.3 ppm downfield from H_c. This difference in the chemical shifts indicated for more positive electric-field potential around H_b than around H_c. Because of the identity in the bonding microenvironment around these two protons, the anthranilamide dipole moment was the most plausible source for the difference in the electric potentials around H_b and H_c. Considering that the downfield shift in the H_b signal was consistent with a more positive potential than the potential around H_c, we could assign the direction of the anthranilamide dipole moment to be from the N- to the C-terminus: i.e., the negative pole of the dipole was oriented toward the N-terminus and the positive pole, toward the C-terminus, consistent with the findings from our ab initio theoretical findings.[20]

CONCLUSIONS

Anthranilamides possess intrinsic dipole moments and manifest a large propensity for self-assembly. The estimated dielectric properties of solutions of these conjugates, along with the lack of pronounced dependence of their spectral wavelength features on their molecular size, indicated for codirectional arrangements of these oligomers within their aggregates. NMR data elucidated that the orientation of the intrinsic dipoles is from the N- to the C-termini of the trianthranilamide oligomer. These findings demonstrate the anthranilamides as organic molecular electrets.

EXPERIMENTAL SECTION

Materials. Palladium (10%) on activated carbon powder was purchased from Sigma-Aldrich, and 2-amino-*N*-phenylbenzamide (95%), octanoyl chloride (99%), pyridine (99.5+%), 2-nitrobenzoyl chloride (97%), and all other reagents, including spectroscopic grade and anhydrous solvents dichloromethane (>99.8%) and *N*,*N*-dimethylformamide (DMF, 99.8%), were used as supplied by commercial vendors.

Synthesis. The anthranilamide oligomers were synthesized from the C- to the N-termini by consequential addition of 2-nitrobenzoyl chloride and reduction of the nitro groups to amines, preparing it for the next coupling step.[21] We started with 2-amino-*N*-phenylbenzamide as a phenyl-capped N-terminus.

General Information. Proton (^{1}H) NMR spectra were recorded at 400 MHz at ambient temperature using $CDCl_3$ as solvent unless otherwise stated. Chemical shifts are reported in parts per million relative to $CDCl_3$ (^{1}H, δ 7.24; ^{13}C, δ 77.23). Data for ^{1}H NMR are reported as follows: chemical shift, integration, multiplicity (s = singlet, d = doublet, t = triplet, q = quartet, m = multiplet), integration and coupling constants. High-resolution mass-spectra were obtained on a Q-TOF mass spectrometer.[61] Analytical thin layer chromatography was performed using 0.25 mm silica gel 60-F plates. Flash chromatography was performed using 60 Å, 32−63 μm silica gel. Yields refer to chromatographically and spectroscopically pure materials, unless otherwise stated.[62] All reactions were carried out in oven-dried glassware under an argon atmosphere unless otherwise noted.

The purity of the anthranilamide oligomers was examined using TLC (normal phase), HPLC−MS (reverse phase) and melting point. For the HPLC tests, the mobile phase, 10% to 98% acetonitrile in water (+0.1% trifluoroacetic acid), was applied as linear gradients between 0.5 and 2 mL min^{-2}, at flow rate 0.9 mL min^{-1}. The stationary phase in the column was 3 μm C8(2), 100 Å, packed in a 30 × 3.00 mm column (Phenomenex Luna). Melting points were recorded using an electrothermal capillary melting point apparatus and are uncorrected. Combustion elemental analysis for carbon, hydrogen and nitrogen was conducted by Atlantic Microlab, Inc. (Norcross, GA). The samples were dried in vacuo for 2−4 h prior to the analysis. The weight percentages for carbon, hydrogen, and nitrogen were reported. The expected values for the weight percentages were calculated from the empirical formulas using the known atomic weights.[63]

2-Octanamido-N-phenylbenzamide (h-A-Ph). To an ice-chilled 10 mL CH_2Cl_2 solution of 2-amino-*N*-phenylbenzamide (200 mg, 0.94 mmol) and pyridine (190 mg, 0.20 mL, 2.4 mmol) was added octanoyl chloride (310 mg, 1.9 mmol). The mixture was stirred at 0 °C to room temperature for 2 h. The reaction mixture was diluted with 50 mL of CH_2Cl_2 and then washed with 1 N HCl (50 mL × 2), saturated $NaHCO_3$ (70 mL), and brine (50 mL). The organic layer was dried over Na_2SO_4 and concentrated in vacuo to afford white powder. Purification via flash chromatography on silica gel (100% CH_2Cl_2 to 1% MeOH in CH_2Cl_2) afforded 300 mg (0.88 mmol, 94%) of h-A-Ph (CAS no. 881768-10-1): white solid; mp 115−118 °C; ^{1}H NMR (400 MHz, $CDCl_3$) δ 10.65 (1 H, s), 8.55 (1 H, d, J = 8.4 Hz), 8.04 (1 H, s), 7.57 (3 H, t, J = 8.4 Hz), 7.45 (1 H, t, J = 8.4 Hz), 7.39 (2 H, t, J = 7.6 Hz), 7.19 (1 H, td, J = 7.6, 1.2 Hz), 7.08 (1 H, t, J = 7.6 Hz), 2.36 (2 H, t, J = 7.2 Hz), 1.70 (2 H, m), 1.40−1.20 (8 H, m), 0.84 (3 H, t, 7.2 Hz) ppm; ^{13}C NMR (100 MHz, $CDCl_3$) δ 172.69, 167.56, 139.41, 137.73, 132.73, 129.41, 127.09, 125.27, 122.99, 122.19, 121.65, 120.92, 38.63, 31.90, 29.43, 29.23, 25.70, 22.82, 14.28 ppm; HRMS m/z calcd for $C_{21}H_{26}N_2O_2Na$ (M + Na) 361.1892, found 361.1891 (M + Na). Anal. Calcd for $C_{21}H_{26}N_2O_2$: C, 74.52; H, 7.74; N, 8.28. Found: C, 74.52; H, 7.74; N, 8.30.

2-Nitro-N-(2-(phenylcarbamoyl)phenyl)benzamide. To an ice-chilled 100 mL CH_2Cl_2 solution of 2-amino-*N*-phenylbenzamide (5.0 g, 24 mmol) and pyridine (4.7 g, 4.8 mL, 59 mmol) was added 2-nitrobenzoyl chloride (8.7 g, 47 mmol). The mixture was stirred at 0 °C to room temperature for 2 h. The reaction mixture was diluted with 500 mL of CH_2Cl_2 and then washed with 1 N HCl (300 mL × 2), saturated $NaHCO_3$ (300 mL), and brine (300 mL). The organic layer was dried over Na_2SO_4, and concentrated in vacuo to afford a white solid (8.1 g, 22 mmol, 95%): ^{1}H NMR (400 MHz, $CDCl_3$) δ 11.30 (1 H, s), 8.71 (1 H, d, J = 8.4 Hz), 8.04 (1 H, d, J = 8.0 Hz), 7.93 (1 H, s), 7.66 (3 H, m), 7.57 (2 H, m), 7.50 (2 H, t, J = 8.0 Hz), 7.36 (2 H, td, J = 8, 1.2 Hz), 7.19 (3 H, m) ppm.

2-Octanamido-N-(2-(phenylcarbamoyl)phenyl)benzamide (h-AA-Ph). A 45 mL DMF solution of 2-nitro-*N*-(2-(phenylcarbamoyl)-phenyl)benzamide (5.0 g, 14 mmol) was hydrogenated in the presence of 10% Pd/C (0.44 g) at 1 atm room temperature for 18 h. The reaction mixture was filtered through Celite. CH_2Cl_2 (300 mL0 was

added to the filtrate, which was washed with saturated $NaHCO_3$ (100 mL) and brine (100 mL). The organic layer was dried over Na_2SO_4 and then concentrated in vacuo to afford 2-amino-*N*-(2-(phenylcarbamoyl)phenyl)benzamide as a brown solid (3.7 g). This compound was used in the next step without any further purification.

To a 10 mL DMF solution of 2-amino-*N*-(2-(phenylcarbamoyl)-phenyl)benzamide (1.0 g) and pyridine (0.6 mL, 7.4 mmol) was added 20 mL of CH_2Cl_2 solution octanoyl chloride (1.0 g, 6.0 mmol). The mixture was stirred at room temperature for 2 h. The reaction mixture was diluted with 100 mL of CH_2Cl_2 and then washed with 1 N HCl (50 mL × 2), saturated $NaHCO_3$ (70 mL), and brine (50 mL). The organic layer was dried over Na_2SO_4, and concentrated in vacuo to afford white powder. Purification via flash chromatography on silica gel (100% CH_2Cl_2 to 5% MeOH in CH_2Cl_2) afforded 1.2 g (2.6 mmol, 70% overall yield for the two steps) of h-AA-Ph: white solid; mp 169−171 °C; ^{1}H NMR (400 MHz, $CDCl_3$) δ 11.81 (1 H, s), 11.20 (1 H, s), 8.66 (2 H, dd, J = 8.0, 8.8 Hz), 7.98 (1 H, s), 7.80 (1 H, d, J = 8.0 Hz), 7.67 (1 H, d, J = 7.6 Hz), 7.57 (3 H, m), 7.49 (1 H, t, J = 7.6 Hz), 7.39 (2 H, t, J = 8.0 Hz), 7.22 (3 H, m), 2.40 (2 H, t, J = 8.0 Hz), 1.72 (2 H, m), 1.40−1.20 (8 H, m), 0.84 (3 H, t, J = 6.4 Hz) ppm; ^{13}C NMR (100 MHz, $CDCl_3$) δ 172.42, 168.08, 167.50, 140.72, 139.47, 137.28, 133.37, 133.15, 129.46, 127.50, 127.05, 125.62, 123.91, 123.32, 122.50, 121.99, 121.65, 121.14, 120.23, 38.88, 31.90, 29.41, 29.22, 25.79, 22.82, 14.28 ppm; HRMS m/z calculated for $C_{28}H_{31}N_3O_3Na$ (M + Na) 480.2263, found 480.2284 (M + Na). Anal. Calcd for $C_{28}H_{31}N_3O_3$: C, 73.50; H, 6.83; N, 9.18. Found: C, 72.60; H, 6.64; N, 9.00.

2-Octanamido-N-(2-((2-(phenylcarbamoyl)phenyl)carbamoyl)-phenyl)benzamide (h-AAA-Ph). To 25 mL DMF solution of 2-amino-*N*-(2-(phenylcarbamoyl)phenyl)benzamide (2.5 g, 7.5 mmol) and pyridine (1.5 mL, 19 mmol) was added 15 mL of DMF solution of 2-nitrobenzoyl chloride (2.8 g, 15 mmol). The mixture was stirred at room temperature for 3 h. A large amount of white solid precipitated out. The solid was collected by filtration and then washed with 1 N HCl, saturated $NaHCO_3$, and water. The dried solid, 2-nitro-*N*-(2-((2-(phenylcarbamoyl)phenyl)carbamoyl)phenyl)benzamide (2.2 g), was used directly for the next step without further purification.

A DMF solution (50 mL) of 2-nitro-*N*-(2-((2-(phenylcarbamoyl)-phenyl)carbamoyl)phenyl)benzamide (2.2 g, 4.6 mmol) was hydrogenated in the presence of 10% Pd/C (0.5 g) at 1 atm room temperature for 48 h. The reaction mixture was filtered through Celite. CH_2Cl_2 (500 mL) was added to the filtrate, which was washed with saturated $NaHCO_3$ (200 mL) and brine (200 mL). The organic layer was dried over Na_2SO_4 and then concentrated in vacuo to afford 2-amino-*N*-(2-((2-(phenylcarbamoyl)phenyl)carbamoyl)phenyl)-benzamide as brown solid (0.8 g). This compound was used in the next step without any further purification.

To a 15 mL DMF solution of 2-amino-*N*-(2-((2-(phenylcarbamoyl)phenyl)carbamoyl)phenyl) benzamide (0.5 g, 1.1 mmol) and pyridine (0.2 g, 0.2 mL, 2.7 mmol) was added octanoyl chloride (0.36 g, 2.2 mmol). The mixture was stirred at room temperature for 3 h. The reaction mixture was diluted with 150 mL of CH_2Cl_2 and washed with 1 N HCl (70 mL × 2), saturated $NaHCO_3$ (100 mL), and brine (70 mL). The organic layer was dried over Na_2SO_4 and concentrated in vacuo to afford white powder. Purification via flash chromatography on silica gel (100% CH_2Cl_2 to 10% MeOH in CH_2Cl_2) afforded 0.48 g (0.8 mmol, 18% overall yield for the three steps) of h-AAA-Ph: white solid; mp 198−200 °C; ^{1}H NMR (400 MHz, $CDCl_3$) δ 12.23 (1 H, s), 11.93 (1 H, s), 11.19 (1 H, s), 8.66 (2 H, m), 8.04 (1 H, s), 7.87 (2 H, t, J = 9.2 Hz), 7.65 (1 H, d, J = 8.0 Hz), 7.57 (4 H, m), 7.45 (1 H, t, J = 8.0 Hz), 7.28 (2 H, t, J = 7.6 Hz), 7.20 (4 H, m), 2.39 (2 H, t, J = 8.0 Hz), 1.71 (2 H, m, J = 7.6 Hz), 1.40−1.20 (8 H, m), 0.84 (3 H, t, 6.4 Hz) ppm; ^{13}C NMR (100 MHz, $CDCl_3$) δ 172.5, 168.0, 167.9, 167.6, 140.6, 140.1, 139.1, 137.4, 133.3, 133.1, 133.0, 132.7, 129.5, 127.8, 127.3, 127.2, 125.6, 124.3, 124.0, 123.2, 122.5, 122.1, 122.0, 121.7, 121.3, 120.8, 38.8, 31.9, 29.4, 29.2, 25.7, 22.8, 14.3 ppm; HRMS m/z calcd for $C_{35}H_{37}N_4O_4$ (M + H) 577.2815, found 577.2819 (M + H). Anal. Calcd for $C_{35}H_{36}N_4O_4$: C, 72.90; H, 6.29; N, 9.72. Found: C, 72.87; H, 6.23; N, 9.77.

Absorption and Emission UV/Visible Spectroscopy. Steady-state UV/Visible absorption spectra were recorded in a transmission mode. Steady-state and time-resolved emission measurements were conducted using a spectrofluorometer with double-grating monochromators and a single-photon-counting detector.[64,65] For steady-state emission measurement, a long-pass glass filter was placed on the emission pathway to prevent the appearance of Rayleigh scattered excitation light at 2 × λ_{ex}.[39,40,66] For time-resolved emission measurements, a NanoLED was used for an excitation source (λ_{ex} = 278 nm; half-height pulse width, $W_{1/2}$ = 1 ns). For recording the profile of the excitation pulse (i.e., the instrument response function), we used deionized water as a scatterer, setting $\lambda_{em} = \lambda_{ex}$ = 278 nm. The fluorescence decays of anthranilamides were recorded at two emission maxima, high-energy bands (λ_{em} = 400 nm for all three anthranilamides), and red-shifted bands (λ_{em} = 545 nm for h-A-ph, λ_{em} = 520 nm for h-AA-ph and h-AAA-ph).

The fluorescence quantum yields, Φ, for different concentrations of the anthranilamide oligomers in chloroform were determined by comparing the integrated emission intensities of the samples with the integrated fluorescence of a reference sample with a known fluorescence quantum yield, Φ_0.[36,64,67] Extrapolations to zero and to infinity concentrations yielded, respectively, the estimates for the quantum yields of the monomeric and aggregated forms of the oligomers. For references, we used solutions of coumarin 151 in ethanol (Φ_0 = 0.49) and phenanthrene in ethanol (Φ_0 = 0.13).[68−72]

Dielectric Measurements. We followed procedures as described previously to calculate the dielectric values.[23] Three-terminal capacitance sample cell connected to an ultrahigh precision Wheatstone bridge, incorporated into a precision meter via connecting cables with up to of 4 m length were used to collect capacitance data. The three-terminal sample cell electrodes were separated to 400 μm and filled with 1.5 mL of freshly prepared sample solution. The capacitance measurements were carried at frequencies ranging from 10^4 to 10^6 Hz. The capacitance of the neat solvent and of air was measured in an empty dry cell as controls.[23]

The experimentally determined dielectric values presented in the tables and figures correspond to averages of at least five repeats, where the error bars represent plus/minus one standard deviation.

Density Measurements. The densities of freshly prepared anthranilamide solutions were measured with a calibrated portable density meter, recorded at 21 °C (± 0.5 °C). Before and after each measurement, the densitometer was washed several times with neat solvent, nitrogen dried, and washed with the corresponding sample solution.

■ ASSOCIATED CONTENT

Ⓢ Supporting Information

Copies of ^{13}C NMR spectra of h-A-ph, h-AA-ph, and h-AAA-ph. This material is available free of charge via the Internet at http://pubs.acs.org.

■ AUTHOR INFORMATION

Corresponding Author

*Tel: 951-827-6239. Fax: 951-827-6416. E-mail: vullev@ucr.edu.

Present Address

#GlaxoSmithKline, (MDR-Boston), 830 Winter St, Waltham, MA 02451.

Notes

The authors declare no competing financial interest.

■ ACKNOWLEDGMENTS

This work was supported by the National Science Foundation (CBET 0935995 and CBET 0923408), the Riverside Public Utilities, and the American Public Power Association (Demonstration of Energy-Efficient Developments student

research grant, awarded to S.U.). We thank Dr. Shugeng Cao (Harvard Medical School) and Dr. Yu Chen and Dr. Xiang Liu (Boston University) for helpful discussions.

REFERENCES

(1) Kepler, R. G. *Annu. Rev. Phys. Chem.* **1978**, *29*, 497−518.
(2) Erhard, D. P.; Lovera, D.; von Salis-Soglio, C.; Giesa, R.; Altstaedt, V.; Schmidt, H.-W. *Adv. Polym. Sci.* **2010**, *228*, 155−207.
(3) Suzuki, Y. *IEEJ Trans. Electr. Electron. Eng.* **2011**, *6*, 101−111.
(4) Vullev, V. I. *J. Phys. Chem. Lett.* **2011**, *2*, 503−508.
(5) Garcia, H. *J Phys Chem Lett* **2011**, *2*, 520−521.
(6) Hol, W. G. J.; Van Duijnen, P. T.; Berendsen, H. J. C. *Nature* **1978**, *273*, 443−446.
(7) Shin, Y.-G. K.; Newton, M. D.; Isied, S. S. *J. Am. Chem. Soc.* **2003**, *125*, 3722−3732.
(8) Doyle, D. A.; Cabral, J. M.; Pfuetzner, R. A.; Kuo, A. L.; Gulbis, J. M.; Cohen, S. L.; Chait, B. T.; MacKinnon, R. *Science* **1998**, *280*, 69−77.
(9) Dutzler, R.; Campbell, E. B.; Cadene, M.; Chait, B. T.; MacKinnon, R. *Nature* **2002**, *415*, 287−294.
(10) Galoppini, E.; Fox, M. A. *J. Am. Chem. Soc.* **1996**, *118*, 2299−2300.
(11) Fox, M. A.; Galoppini, E. *J. Am. Chem. Soc.* **1997**, *119*, 5277−5285.
(12) Yasutomi, S.; Morita, T.; Imanishi, Y.; Kimura, S. *Science* **2004**, *304*, 1944−1947.
(13) Jones, G., II; Zhou, X.; Vullev, V. I. *Photochem. Photobiol. Sci.* **2003**, *2*, 1080−1087.
(14) Gray, H. B.; Winkler, J. R. *Proc. Nat. Acad. Sci. U.S.A.* **2005**, *102*, 3534−3539.
(15) Beratan, D. N.; Onuchic, J. N.; Winkler, J. R.; Gray, H. B. *Science* **1992**, *258*, 1740−1741.
(16) Vullev, V. I.; Jones, G., II. *Res. Chem. Intermed.* **2002**, *28*, 795−815.
(17) Jones, G., II; Vullev, V.; Braswell, E. H.; Zhu, D. *J. Am. Chem. Soc.* **2000**, *122*, 388−389.
(18) Jones, G., II; Lu, L. N.; Vullev, V.; Gosztola, D.; Greenfield, S.; Wasielewski, M. *Bioorg. Med. Chem. Lett.* **1995**, *5*, 2385−2390.
(19) Shih, C.; Museth, A. K.; Abrahamsson, M.; Blanco-Rodriguez, A. M.; Di Bilio, A. J.; Sudhamsu, J.; Crane, B. R.; Ronayne, K. L.; Towrie, M.; Vlcek, A., Jr.; Richards, J. H.; Winkler, J. R.; Gray, H. B. *Science* **2008**, *320*, 1760−1762.
(20) Ashraf, M. K.; Pandey, R. R.; Lake, R. K.; Millare, B.; Gerasimenko, A. A.; Bao, D.; Vullev, V. I. *Biotechnol. Prog.* **2009**, *25*, 915−922.
(21) Hamuro, Y.; Geib, S. J.; Hamilton, A. D. *J. Am. Chem. Soc.* **1996**, *118*, 7529−7541.
(22) Hamuro, Y.; Hamilton, A. D. *Bioorg. Med. Chem.* **2001**, *9*, 2355−2363.
(23) Upadhyayula, S.; Bao, D.; Millare, B.; Sylvia, S. S.; Habib, K. M. M.; Ashraf, K.; Ferreira, A.; Bishop, S.; Bonderer, R.; Baqai, S.; Jing, X.; Penchev, M.; Ozkan, M.; Ozkan, C. S.; Lake, R. K.; Vullev, V. I. *J. Phys. Chem. B* **2011**, *115*, 9473−9490.
(24) Gong, B. *Acc. Chem. Res.* **2008**, *41*, 1376−1386.
(25) Zhu, J.; Wang, X.-Z.; Chen, Y.-Q.; Jiang, X.-K.; Chen, X.-Z.; Li, Z.-T. *J. Org. Chem.* **2004**, *69*, 6221−6227.
(26) Colombo, S.; Coluccini, C.; Caricato, M.; Gargiulli, C.; Gattuso, G.; Pasini, D. *Tetrahedron* **2010**, *66*, 4206−4211.
(27) Coluccini, C.; Mazzanti, A.; Pasini, D. *Org. Biomol. Chem.* **2010**, *8*, 1807−1815.
(28) Wan, J.; Thomas, M. S.; Guthrie, S.; Vullev, V. I. *Ann. Biomed. Eng.* **2009**, *37*, 1190−1205.
(29) Upadhyayula, S.; Quinata, T.; Bishop, S.; Gupta, S.; Johnson, N. R.; Bahmani, B.; Bozhilov, K.; Stubbs, J.; Jreij, P.; Nallagatla, P.; Vullev, V. I. *Langmuir* **2012**, *28*, 5059−5069.
(30) Ghazinejad, M.; Kyle, J. R.; Guo, S.; Pleskot, D.; Bao, D.; Vullev, V. I.; Ozkan, M.; Ozkan, C. S. *Adv. Funct. Mater.* **2012**, *22*, 4519−4525.
(31) Lu, H.; Bao, D.; Penchev, M.; Ghazinejad, M.; Vullev, V. I.; Ozkan, C. S.; Ozkan, M. *Adv. Sci. Lett.* **2010**, *3*, 101−109.
(32) Thomas, M. S.; Clift, J. M.; Millare, B.; Vullev, V. I. *Langmuir* **2010**, *26*, 2951−2957.
(33) Mayers, B. T.; Vezenov, D. V.; Vullev, V. I.; Whitesides, G. M. *Anal. Chem.* **2005**, *77*, 1310−1316.
(34) Jones, G., II; Vullev, V. I. *J. Phys. Chem. A* **2001**, *105*, 6402−6406.
(35) Vullev, V. I.; Jiang, H.; Jones, G., II. *Top. Fluoresc. Spectrosc.* **2005**, *10*, 211−239.
(36) Valeur, B. *Molecular Fluorescence, Principles and Applications*; Wiley-VCH: New York, 2002.
(37) Vasquez, J. M.; Vu, A.; Schultz, J. S.; Vullev, V. I. *Biotechnol. Prog.* **2009**, *25*, 906−914.
(38) Jones, G., II; Vullev, V. I. *Org. Lett.* **2001**, *3*, 2457−2460.
(39) Jones, G., II; Vullev, V. I. *J. Phys. Chem. A* **2002**, *106*, 8213−8222.
(40) Jones, G., II; Vullev, V. I. *Photochem. Photobiolog. Sci.* **2002**, *1*, 925−933.
(41) Jones, G., II; Vullev, V. I. *Org. Lett.* **2002**, *4*, 4001−4004.
(42) Vullev, V. I.; Jones, G. *Tetrahedon. Lett.* **2002**, *43*, 8611−8615.
(43) Eaton, D. F. *Pure Appl. Chem.* **1990**, *62*, 1631−1648.
(44) Hisamatsu, H.; Maekawa, K. *J. Econometrics* **1994**, *61*, 367−382.
(45) Rutledge, D. N.; Barros, A. S. *Anal. Chim. Acta* **2002**, *454*, 277−295.
(46) Xia, B.; Upadhyayula, S.; Nuñez, V.; Landsman, P.; Lam, S.; Malik, H.; Gupta, S.; Sarshar, M.; Hu, J.; Anvari, B.; Jones, G.; Vullev, V. I. *J. Clin. Microbiol.* **2011**, *49*, 2966−2975.
(47) Bao, D.; Millare, B.; Xia, W.; Steyer, B. G.; Gerasimenko, A. A.; Ferreira, A.; Contreras, A.; Vullev, V. I. *J. Phys. Chem. A* **2009**, *113*, 1259−1267.
(48) Bao, D.; Ramu, S.; Contreras, A.; Upadhyayula, S.; Vasquez, J. M.; Beran, G.; Vullev, V. I. *J. Phys. Chem. B* **2010**, *114*, 14467−14479.
(49) Hedestrand, G. *Z. Physik. Chem.* **1929**, *2*, 428−444.
(50) Debye, P. J. W. Polar *Molecules*; Dover Publications, Inc.: New York, 1945.
(51) Böttcher, C. J. F. *Theory of Electric Polarization*, 2nd ed.; Elsevier Scientific Publishing Co.: New York, 1973; Vol. *I*, Dielectrics Static Fields.
(52) Böttcher, C. J. F.; Bordewijk, P. *Theory of Electric Polarization*; Elsevier Scientific Publishing Co.: New York, 1978; Vol. *II*, Dielectrics in Time-Dependent Fields.
(53) Hill, N. E.; Vaughan, W. E.; Price, A. H.; Davies, M. *Dielectric Properties and Molecular Behavior (The Van Nostrand Series in Physical Chemistry)*; Van Nostrand Reinhold Co. Ltd.: New York, 1969.
(54) Breitung, E. M.; Vaughan, W. E.; McMahon, R. J. *Rev. Sci. Instrum.* **2000**, *71*, 224−227.
(55) Tjahjono, M.; Davis, T.; Garland, M. *Rev. Sci. Instrum.* **2007**, *78*, 023902/023901−023902/023906.
(56) Hong, C.; Bao, D.; Thomas, M. S.; Clift, J. M.; Vullev, V. I. *Langmuir* **2008**, *24*, 8439−8442.
(57) Hu, J.; Xia, B.; Bao, D.; Ferreira, A.; Wan, J.; Jones, G.; Vullev, V. I. *J. Phys. Chem. A* **2009**, *113*, 3096−3107.
(58) Araya-Maturana, R.; Pessoa-Mahana, H.; Weiss-Lopez, B. *Nat. Prod. Commun.* **2008**, *3*, 445−450.
(59) Martins, J. C.; Biesemans, M.; Willem, R. *Prog. Nucl. Magn. Reson. Spectrosc.* **2000**, *36*, 271−322.
(60) Lockhart, D. J.; Kim, P. S. *Science* **1993**, *260*, 198−202.
(61) Wu, J.; Becerril, J.; Lian, Y.; Davies, H. M. L.; Porco, J. A.; Panek, J. S. *Angew. Chem., Int. Ed.* **2011**, *50*, 5938−5942.
(62) Jones, G., II; Yan, D.; Hu, J.; Wan, J.; Xia, B.; Vullev, V. I. *J. Phys. Chem. B* **2007**, *111*, 6921−6929.
(63) Wieser, M. E.; Coplen, T. B. *Pure Appl. Chem.* **2011**, *83*, 359−396.
(64) Wan, J.; Ferreira, A.; Xia, W.; Chow, C. H.; Takechi, K.; Kamat, P. V.; Jones, G.; Vullev, V. I. *J. Photochem. Photobiol. A* **2008**, *197*, 364−374.
(65) Bahmani, B.; Gupta, S.; Upadhyayula, S.; Vullev, V. I.; Anvari, B. *J. Biomed. Optics* **2011**, *16*, 051303/051301−051303/051310.

(66) Vullev, V. I.; Wan, J.; Heinrich, V.; Landsman, P.; Bower, P. E.; Xia, B.; Millare, B.; Jones, G., II. *J. Am. Chem. Soc.* **2006**, *128*, 16062−16072.
(67) Demas, J. N.; Crosby, G. A. *J. Phys. Chem.* **1971**, *75*, 991−1024.
(68) Nad, S.; Pal, H. *J. Phys. Chem. A* **2001**, *105*, 1097−1106.
(69) Thomas, M. S.; Nuñez, V.; Upadhyayula, S.; Zielins, E. R.; Bao, D.; Vasquez, J. M.; Bahmani, B.; Vullev, V. I. *Langmuir* **2010**, *26*, 9756−9765.
(70) Montalti, M.; Credi, A.; Prodi, L.; Gandolfi, M. T. *Handbook of Photochemistry*, 3rd ed.; CRC Press: Boca Raton, 2006.
(71) Brouwer, A. M. *Pure Appl. Chem.* **2011**, *83*, 2213−2228.
(72) Dawson, W. R.; Windsor, M. W. *J. Phys. Chem.* **1968**, *72*, 3251−3260.